I.J. Image, Graphics and Signal Processing, **2025, 4, 14-32**
Published Online on August 8, 2025 by MECS Press (http://www.mecs-press.org/)
DOI: 10.5815/ijigsp.2025.04.02

Computed Tomography Image Segmentation Technology Based on ResNet Network Integrated into the Probabilistic Model

Zhengbing Hu
School of Computer Science, Hubei University of Technology, Wuhan, China
E-mail: drzbhu@gmail.com
ORCID iD: https://orcid.org/0000-0002-6140-3351

Kostiantyn Zvieriev*
Department of Computer Systems Software, Igor Sikorsky Kyiv Polytechnic Institute, Kyiv, 03056, Ukraine
E-mail: zvieriev.kostiantyn@outlook.com
ORCID iD: https://orcid.org/0009-0007-1265-5927
*Corresponding Author

Oksana Shkurat
Department of Computer Systems Software, Igor Sikorsky Kyiv Polytechnic Institute, Kyiv, 03056, Ukraine
E-mail: shkurat@pzks.fpm.kpi.ua
ORCID iD: https://orcid.org/0000-0001-7633-9121

Andrii Dychka
Department of Computer Systems Software, Igor Sikorsky Kyiv Polytechnic Institute, Kyiv, 03056, Ukraine
E-mail: andriydychka@gmail.com
ORCID iD: https://orcid.org/0000-0003-0578-2788

Received: 01 February, 2025; Revised: 12 March, 2025; Accepted: 15 May, 2025; Published: 08 August, 2025

Abstract: Medical image segmentation is a significant and complex challenge in medical imaging. In recent years, deep learning models have been applied to image segmentation and have shown exceptional performance. However, medical image segmentation has a scarcity of expert-labeled data compared to other deep learning research fields. Therefore, augmenting medical expert-labeled data are primarily the easiest and fastest way to improve the deep learning model's performance. In this paper, computed tomography image segmentation technology based on the ResNet network integrated into the probabilistic model has been proposed. The proposed segmentation technology is based on the deep learning model of the ResNet50 architecture to extract features from images and initially detect objects of interest and on the probabilistic model with weighted parameters that employs conditional random fields, the GrabCut algorithm, and the argmax function to perform the final detection of objects of interest.

To train, test, and evaluate the effectiveness of the proposed method, appropriate chest CT datasets were identified to solve the task of segmenting the lung cavity, the liver and areas affected by COVID-19. The proposed image segmentation technology demonstrates segmentation accuracy results of 73.12% by Dice Score for the COVID-19 disease dataset, 97.71% for the lung cavity dataset, and 98.36% for the liver dataset, which perform better than state-of-the-art solutions.

The proposed image segmentation technology has been compared with state-of-the-art technologies (SegNet, UNet, and FCN-ResNet50) for CT segmentation to demonstrate the effectiveness of the method. The positive outcomes strongly suggest the significant potential of the proposed image segmentation technology. According to the obtained results, the proposed image segmentation technology can be a useful auxiliary tool for doctors to segment CT images for further analysis and monitoring of statistical and dynamic indicators.

Index Terms: Image Segmentation, Deep Residual Network, Atrous Spatial Pyramid Pooling, Conditional Random Fields, GrabCut, Histogram Equalization

1. Introduction

Healthcare professionals use computed tomography (CT) imaging as a diagnostic tool to visualize internal body structures and assess various clinical conditions. Image segmentation is an image processing and analysis technology employed in computed tomography for the informational support in clinical condition evaluation. CT images visualize the inside structures of patients with different genders, ages, etc. There are no universal approaches to image segmentation, and each task is characterized by a segmentation object and application field. The complexity of CT image segmentation is based on the contour overlay of inside structures, their anatomic differences, inhomogeneity in uniform structures, differences in hardware visualization, etc. Developing a CT image segmentation technology that is resistant to noise and data inhomogeneity is a current challenge.

Deep learning, especially through the ongoing development of convolutional neural networks (CNNs) and their variations (UNet [1], DeepLab [2], SegNet [3], ResNet [4], GCN [5], FCN [6], TransUNet [7], SwinUNet [8]), has emerged as an effective image segmentation technology in recent years and continues to be active. CNN models apply sequences of convolutional layers in the encoder to extract timage features, and then apply sequences of deconvolutional layers in the decoder to reconstruct the segmented image. Although CNN models segment an image with a high accuracy rate, three general approaches are used to improve deep learning technology. These are preprocessing the initial images [9-11], modifying the network architectures and attributes [12-16], and less commonly used post-processing the network results [17-18].

In this paper, the mentioned problems of CT image segmentation are considered, along with a proposed segmentation technology based on the ResNet architecture. The main contributions are the following three points:

1. The deep learning model for the ResNet50 network has been constructed to extract features from CT images and detect objects. The ResNet50 network is based on the Compound Pooling block, which is used after early layers of the network feature conventional convolutional and pooling layers to preprocess the image and further processing by the residual blocks. This allows for solving issues of losing image spatial information and relationships, which are critical for medical image analysis.

The deep learning model has been trained on processed CT images. Histogram-based image processing techniques, contrast stretching, noising, geometric transformations, etc., have been applied to CT images. This allows the construction of a general model with the ability to recognize individual details of an image.

2. The probabilistic model with weighted parameters that implements knowledge integration from the sequence of segmented images has been developed to finally detect objects of interest. The probabilistic model employs the argmax function, conditional random fields, and the GrabCut algorithm on a ResNet50 segmented image.

3. The Contextual Block has been constructed based on the probabilistic model. The block enables the capture of local features of the objects in a segmented ResNet50 image and the relationships between neighboring pixels.

This paper is structured as follows. Section 2 details the CT image segmentation studies and technologies. Section 3 describes the proposed CT image segmentation technology based on the ResNet architecture. Section 4 describes the dataset used, experimental results of the proposed technology, and state-of-the-art segmentation technologies. Section 5 provides the conclusion and discusses future research.

2. Related Works

Two main approaches are used to solve the problem of semantic segmentation of images, including medical CT images, namely methods with and without deep learning technologies. Digital image processing-based segmentation is performed quickly and accurately detects the object of interest from an image. This segmentation is effective for object types characterized by complex geometric shapes and can be performed for further multi-class object recognition in more complex computer vision systems. There are many methods of digital image processing-based segmentation for CT images, including threshold segmentation [19-20], region-based segmentation [21-22], clustering segmentation [23-25, 27-28], and edge detection segmentation [27, 29].

Zhou et al. [21] proposed a semi-automatic liver segmentation method on low-contrast CT images by dividing the tissue intensity into five sets and using a region-growing algorithm to form segments. Manually defining the seed points of the liver object and using morphological hole filling reduced the number of segmentation errors in the results by 7%.

Khorshidi et al. [22] applied a modified method for segmenting lung tumors on CT images using an improved region-growing algorithm. Due to the manual restriction of the study area, the method demonstrates better performance, and the sequential division of the study area and interpolation of several results of the method allow for an improvement in the compliance percentage by 13%.

Rim et al. [24] proposed a semantic segmentation method for CT images that is based on combining the K-Means clustering method and the mathematical morphology method. The proposed segmentation method was conducted on 500 different subjects. The overall accuracy achieved 34.90%, and the mean intersection over union achieved 41.26% for image sets that contain full heart scans. These rates are 55.10% and 71.46%, respectively, for image sets that contain half heart scans.

Kong et al. [25] proposed an image segmentation method that is based on an intuitionistic fuzzy C-means clustering algorithm improved by a function to generate the fuzzy set, a method to define initial cluster centers, a distance function, and the fuzzy entropy measure.

Alam et al. [26] implemented a method for detecting brain tumors using superpixels and principal component analysis for the template-based K-means with eight classes on images of magnetic resonance imaging (MRI). Removing noise and unnecessary artifacts by applying a median filter to the input data and morphological operations of dilation and erosion to the principal component features, helped reduce the number of calculations, accelerated the method, and obtained segmentation accuracy and sensitivity at the level of 95.0% and 97.36%, respectively.

Nithila et al. [27] proposed a method for segmenting lung nodules on the LIDC-IDRI dataset based on a region-based active contour model and a 3-class fuzzy C-means technique. Gaussian filtering allowed the speeding up of the method by reducing the number of evolution iterations during lung reconstruction. The average volumetric overlap error (VOE) achieved 0.968% and the under segmentation ratio achieved 0.015%.

Wu et al. [28] proposed a new method for semi-automatic segmentation of liver tumors on contrast-enhanced computed tomography images of the 3Dircadb dataset. The optimization solution is to form an initial region of interest using the confidence-connected region growing algorithm for subsequent intensity-based segmentation using the improved fuzzy C-means and graph cuts algorithms. The results show that the proposed method is fast and has a segmentation accuracy of 83% by Dice Score with a VOE of 12.94%.

Zareei et al. [29] proposed a liver segmentation method based on CT image energy using an active contour model. Using a genetic algorithm to obtain optimal active contour model parameters, it was possible to refine the initial contour of the object. Examining the Sliver CT dataset, the method demonstrates an improvement in segmentation accuracy by 3.5% for Dice Score and a reduction in VOE by 1.4%.

Huang et al. [30] applied an automatic liver segmentation method on low-contrast CT images using a feature detection method to remove redundant vessel anatomical information from the results of the modified graph cut. The proposed solution has a high performance of 12.7s for the 3Dircadb dataset and has a low VOE of 8.6%.

Wang et al. [31] proposed a liver segmentation method for abdominal CT images based on the probability map classification of a probabilistic atlas of liver regions. Despite the low error rate of the VOE method of 7.57% on the considered MICCAI datasets, the method loses segmentation accuracy on samples where the liver tumor area exceeds 35% of the liver area due to the change in intensity and homogeneity of the liver tissues.

Deep learning-based segmentation is performed automatically and detects an object of interest from an image, which can be different due to brightness distribution, noise, object rotation, scale, etc. There are many models of deep learning-based segmentation for CT images, including U-Net [32-34, 36, 43], SegNet [37], and ResUNet [42]. Various adaptive preprocessing and post-processing methods are used in deep learning models. The differences in performance among models and the impact of various adaptive preprocessing and post-processing methods are not clearly defined.

Skourt et al. [32] proposed the use of a U-Net model with a depth of 4 levels for binary lung segmentation on the LIDC-IDRI dataset. By applying a sigmoid activation function in the last convolutional layer and performing 50 training epochs with a batch size of 32, the proposed method demonstrates a high segmentation accuracy of 95% by Dice Score.

Christ et al. [33], [34] applied a cascade of fully convolutional neural networks to segment the liver and its lesions. This combined automatic segmentation method uses 19-layer U-Net models and dense three-dimensional conditional random fields as the last step in forming the segmentation result of low-contrast medical images of CT and MRI. The results demonstrate an increase in segmentation accuracy by 21.4% by Dice Score for the 3DIRCAD dataset.

Sun et al. [35] first implemented an automatic liver tumor segmentation method using a multichannel FCN with 24 convolutional layers. Using the 3Dircab and JDRD datasets of multiphase contrast-enhanced computed tomography images, the authors combined the multi-level network features of individual phases, improving the quality of the corresponding pathological features. According to experimental data, the average values of the VOE are 11.5%.

Cai et al. [36] proposed the use of a U-Net network model with a depth of 4 in combination with the atrous spatial pyramid pooling module, which allowed the authors to expand the sensitivity field of feature extraction and increase the accuracy of spine MRI image segmentation by 7% according to the Dice Score. The work used three dilation convolutions of the atrous spatial pyramid pooling module with the corresponding dilation parameters of 6, 12, and 18, which accelerated the convergence of the network and the loss curve flattened out after 17 training epochs.

Nayantara et al. [37] proposed using a SegNet model with four encoder-decoder pairs and an ASPP module for liver segmentation from the 3D-IRCADb dataset. According to the solution proposed by the authors, the encoder layers are initialized from the weights of a VGG-16 network trained on the ImageNet database; the implementation of the atrous spatial pyramid pooling module resulted in a 1.2% improvement in segmentation accuracy by Dice Score compared to state-of-the-art solutions.

Kamnitsas et al. [38] applied a deep 3D convolutional network model with 11 layers for segmenting brain lesions in multi-modal MRI images. Using a dual pathway architecture for simultaneously processing images at multiple scales, the authors could better account for local and contextual information. Using conditional random fields can reduce the proportion of false-positive segmentation results. Despite the increase in the number of calculations, execution time, and memory, the proposed solution achieved a 5% improvement in segmentation accuracy, according to Dice Score.

Zhang et al. [39] proposed an approach for semantic segmentation of the liver in contrast-enhanced computed tomography images using a symmetric Transformer Encoder-Decoder architecture. Using a proprietary cross-phase feature aggregator allowed the authors to use information from different phases for better generalization and improve the segmentation accuracy by 8%, according to the Dice Score.

Xie et al. [40] implemented a dynamic adaptive network model for liver segmentation in abdominal CT images. The novelty of their solution is the use of interpolation optimization to form more accurate features in the pooling domain and the residual structure to improve the network's generalization ability. By removing irrelevant pixels and integrating conditional random fields, the method improves the segmentation accuracy by 13.02% in terms of Dice Score on the 3DIRCADB.

Dutande et al. [41] first proposed a method for segmenting lung cancer tumors on CT images using a deep residual separable CNN model. Thanks to atrous convolutions and separable convolutional residual units, the network solves the problems of image context loss and high-resolution feature loss. The results of using the method on the StructSeg 2019 datasets demonstrate a high level of accuracy of 64.9% by Dice Score.

Manjunath et al. [42] proposed a method for automated liver segmentation from 3Dircadb images using the ResUNet model. The considered hybrid model is built on U-Net architecture with 49 layers and three residual blocks in the encoder component, providing the ability to segment resized 128x128 images with an accuracy of 93.08% by Dice Score and with a VOE of 12.87%.

Ilhan et al. [43] implemented a method for segmenting affected lung areas on CT images of the COVID-19 dataset using the U-Net model and nonparametric histogram-based region localization and enhancement. The implemented changes increased the informativeness of the regions, and led to a 21% increase in the accuracy of the method's segmentation, as measured by the Dice Score.

In this paper, CT image segmentation technology is proposed, which is based on deep learning-based segmentation and digital image processing-based segmentation and achieves high accuracy of object detection for CT chest images. Deep learning-based segmentation is a general segmentation technology that is resistant to differences in input data and sensitive to training data at the same time. In deep learning-based segmentation methods, the amount of data, their quality, and diversity define the segmentation result directly. Insufficient data in deep learning models leads to overfitting or poor generalization, unstable technology, and, as a result, errors in segmentation. Deep learning-based segmentation is always an automatic technology, is not fast since the cost of training a model exists, and is less accurate with homogeneous data. Digital image processing-based segmentation can be automatic, semi-automatic, or manual. This segmentation is accurate and fast, however sensitive to input data and with poor generalization. In the proposed CT image segmentation technology, deep learning-based segmentation, which is based on the ResNet architecture, is performed to initially detect objects of interest. Digital image processing-based segmentation, which is based on a developed probabilistic model with weighted parameters that employs conditional random fields, the GrabCut algorithm, and the argmax function, is performed to finally detect objects of interest.

3. Method Description

In this section, the proposed segmentation method for CT medical images is considered. The initial dataset is a grayscale image that needs to be segmented into an object of interest and a composed background. A composed background includes the scene background and irrelevant objects. The proposed segmentation method is based on (see Fig. 1):

– Contrast Limited Adaptive Histogram Equalization (CLAHE)
– Deep Learning Model for ResNet50 Network
– Contextual Probabilistic Model.

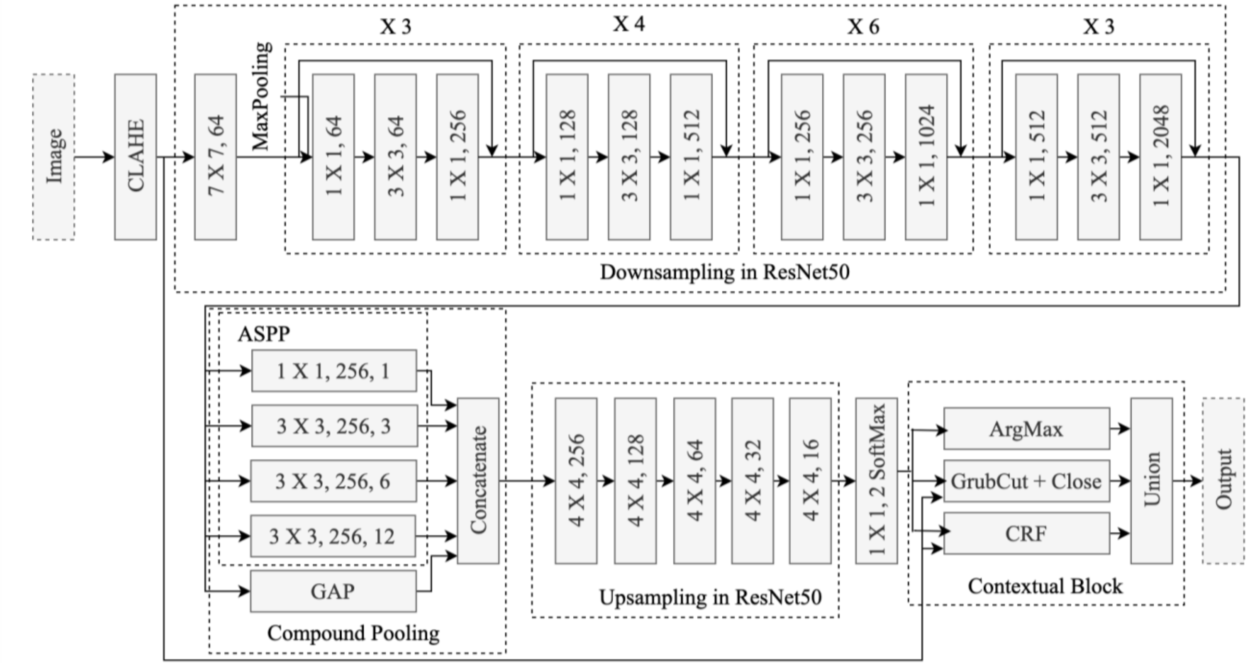

Fig. 1. Architecture of the proposed image segmentation method.

3.1. Contrast Limited Adaptive Histogram Equalization

The initial data are a grayscale image represented by two-dimensional matrix $Image(i, j) = b$, where b is pixel brightness, $b \in [0; 255]$, (i, j) are pixel coordinates, $i = \overline{1, N}, j = \overline{1, N}$, $N \times N$ is image dimension, $N = 512$. A grayscale image of computer tomography is characterized by lower local contrasts when the dark regions contain low contrast and the light regions contain high contrast (see Fig. 2).

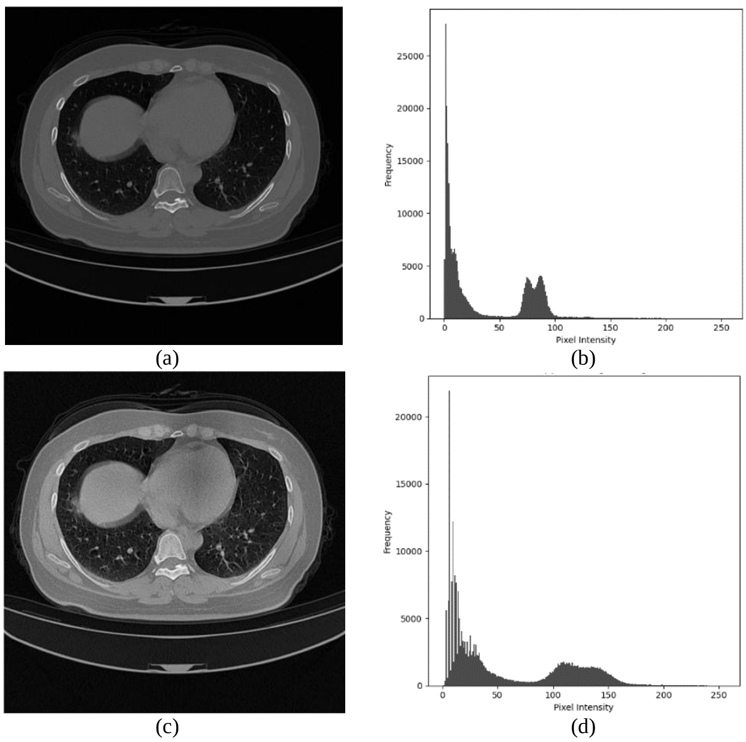

Fig. 2. Image quality enhancement: (a) original image of CT chest; (b) histogram of (a) image; (c) image of CT chest processed by the CLAHE method, threshold of contrast limiting is 2, grid size is 8x8; (d) histogram of (c) image.

At the same time, the global contrast of a CT image is sufficient. Thus, an adaptive method is needed to enhance the image quality, in particular, the contrast limited adaptive histogram equalization (CLAHE) [44] is applied (see Figs. 2, 3).

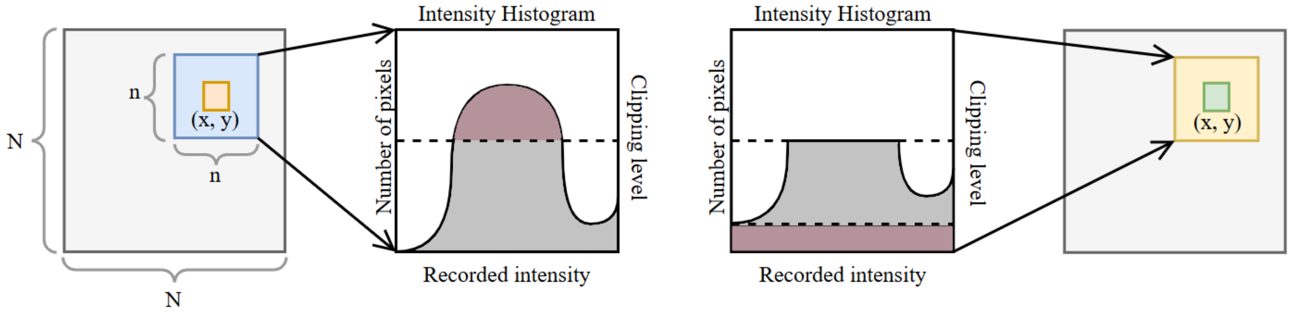

Fig. 3. Contrast Limited Adaptive Histogram Equalization (CLAHE) scheme.

A grayscale image is divided into fragments, to which histogram equalization is applied. Contrast limiting is applied to histograms of image fragments. If a histogram bin of an image fragment is above a threshold of contrast limiting, those pixels are clipped from the initial bin and distributed uniformly to all bins of the image fragment. Equalization is applied to a normalized histogram. Bilinear interpolation is applied to define brightness values for border pixels of image fragments. Finally, image quality enhancement depends on the values of grid size and contrast limiting threshold.

3.2. Deep Learning Model for ResNet50 Network

The ResNet50 network [45], as a deep convolutional neural network, integrates extracted image features and classifiers into an end-to-end multilayer structure for image segmentation. The architecture of the deep learning model for the ResNet50 network is shown in Fig. 1.

Firstly, the max pooling operation after the convolutional layer is applied to reduce the spatial resolution and extract the feature map of a grayscale image.

The residual block extracts the image features and reduces the computational complexity compared to similar deep networks. The series of convolution layers consists of a 1x1 convolutional layer that reduces the dimension, the 3x3 convolutional layer for learning spatial image features, and the 1x1 convolutional layer that restores the dimension. The batch normalization is applied after each convolution layer. The activation function is applied after the first batch normalization and the skip connection. The skip connection is applied at the end of the block and adds the input of the block to the output before the final activation function is applied.

The Compound Pooling block (see Fig. 1) allows accounting for the relationship between image objects. The Compound Pooling block is based on the integration of global average pooling and atrous spatial pyramid pooling (ASPP) (see Fig. 4). Global average pooling (1) sums out the spatial image features, and is more robust to spatial translations of an image. Atrous spatial pyramid pooling computes multi-scale contextual image features (see Fig. 4).

$$Y_{GAP}(c) = \frac{1}{H \times W} \sum_{h=1}^{H} \sum_{w=1}^{W} x(h,w), \quad (1)$$

where x is the value of the feature, (h,w) are feature coordinates, $h = \overline{1,H}, w = \overline{1,W}$, $H \times W$ is feature map dimension,

c is the order number of the feature map, $c = \overline{1,C}$, C is a number of the feature maps.

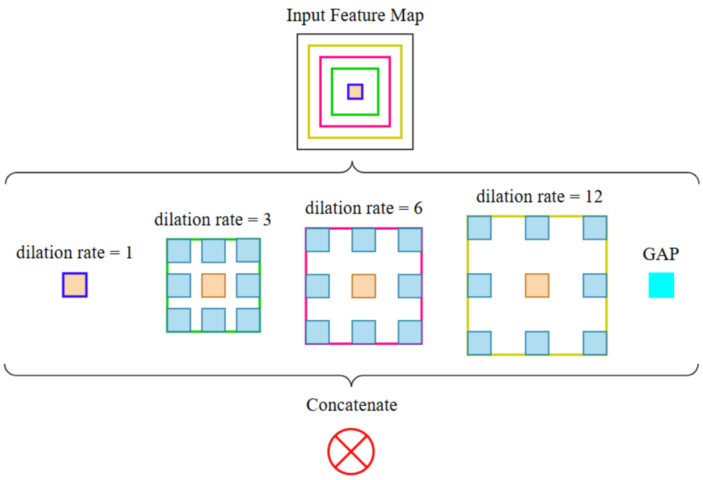

Fig. 4. Atrous Spatial Pyramid Pooling (ASPP) module.

The Compound Pooling block allows combining a global context vector over the entire image map with separate local and remote representations of the context of objects at different scale levels. This feature enables combining more color, texture, and spatial properties of objects, which increases the efficiency of the feature extraction process from the image and also considers the ties between remote objects.

The upsampling block increases the spatial resolution of a segment image and generates a high-resolution image of dimensions 512x512. The upsampling block is based on 5 transposed convolutional layers with a kernel size of 4 and a stride of 2.

Finally, the result of the upsampling block is processed by the convolution layer and softmax function. A segment image provided by the ResNet50 model is a two-dimensional matrix $S(i,j) = p$, where p is the probability of a pixel belonging to a class, $p \in [0;1]$, $i = \overline{1,N}, j = \overline{1,N}$, $N = 512$.

3.3. Contextual Probabilistic Model

Considering the peculiarity of computed tomography images, namely the vagueness of the contours of interacting objects and the complexity of the textural structure of organs and pathologies, the corresponding results of neural network models can form fragmented results that do not contain the necessary information about the contour of objects. In turn, using the CRF method, which considers both the color component of objects and contextual interaction, provides an opportunity to improve the segmentation results and smooth the pixel classes within one object.

To improve the accuracy of a ResNet50 segmented image results, the Contextual Block is used. The Contextual Block is based on a probabilistic model (2) with weighted parameters that employs the argmax function, a Conditional random field, and the GrabCut algorithm to finally detect objects of interest.

$$y_{ji} = k \times y_{ji}^{argmax} + l \times y_{ji}^{CRF} + m \times y_{ji}^{GrabCut}, \tag{2}$$

where k, l, m are the parameters that define the influence of the segmented images on the final result.

The argmax function (3) is applied to a ResNet50 segmented image, that allows forming a segmentation map with $\overline{0,1}$ brightness levels and $N \times N$ size, $N = 512$.

$$argmax_S f := \mathrm{argmax}_{x \in S} f(x) := \{x \in S : f(s) \leq f(x) \text{ for all } s \in S\}. \tag{3}$$

The conditional random fields (CRF) are applied to a ResNet50 segmented image (4), which allows refining the boundaries of objects and considering the local spatial dependence between pixels.

$$E(x) = \sum_i \psi_u(x_i) + \sum_{i<j} \psi_p(x_i, x_j), \tag{4}$$

where $\psi_u(x_i)$ is the unary component, which determines the cost of pixel i receiving the label x_i; $\psi_p(x_i, x_j)$ is the pairwise component, which determines the cost of assigning labels x_i, x_j to corresponding pixels i and j simultaneously.

The unary energy components (5) are obtained from the corresponding SoftMax distribution, which is a somewhat rough estimate that does not take into account the smoothness or consistency of the labels. Since the output of this unary component is computed separately for each pixel and does not take into account the interaction with its neighbors, using it alone will only increase the noise and inconsistency of the data.

$$\psi_u(x_i) = -\log P(x_i), \tag{5}$$

where $P(x_i)$ determines the probability of assigning a label x_i at pixel i in the range [0,1] for background and foreground class, computed by the proposed model.

The pairwise energy component is determined from the corresponding input image to form a smoothing element that encourages the assignment of similar labels to pixels with similar properties. Krähenbühl et al. proposed in [46] to use weighted Gaussians as pairwise potentials, which is an effective solution for multi-class image segmentation that is used in the proposed technology. At the heart of this pairwise component (6) is the sum of two Gaussian kernels: the appearance and smoothness kernel.

$$\psi_p(x_i, x_j) = \mu(x_i, x_j) \cdot [\omega_1 k_a + \omega_2 k_s], \tag{6}$$

where $\mu(x_i, x_j)$ is the function of the label essence according to the Potts model for penalized nodes with different labels, and ω_1, ω_2 are the weights that determine the respective influence of appearance kernel k_a and smoothness kernel k_s on the final result of the pairwise energy component.

The appearance kernel (7) is a bilateral kernel that allows you to determine whether neighboring pixels of the same color belong to the same label.

$$k_a = \exp(-\frac{\|p_i - p_j\|^2}{2\varphi_\alpha^2} - \frac{\|I_i - I_j\|^2}{2\varphi_\beta^2}), \tag{7}$$

where p_i, p_j are the positions of the corresponding color vectors I_i, I_j, and φ_α and φ_β control the degree of their proximity and similarity.

The smoothness kernel (8) depends only on the pixel position, provides spatial smoothness, and removes small isolated areas.

$$k_s = \exp(-\frac{\|p_i - p_j\|^2}{2\varphi_\gamma^2}), \tag{8}$$

where p_i, p_j are the pixel positions, and the parameter φ_γ controls the scale of the Gaussian kernel.

The graph algorithm GrabCut is applied to a ResNet50 segmented image (9), which is based on forming two independent graphs, a background, and a foreground. The data energy indicates how well a pixel matches the foreground or background using color property values and a Gaussian mixture model. The smoothness energy controls the transition between neighboring pixels, encouraging neighboring pixels to belong to the same class if they are similar.

$$E = E_{data} + E_{smooth}, \tag{9}$$

where $E_{data} = \sum_i -\log\left(\sum_{k=1}^{K} \pi_{x_i,k} \cdot \mathcal{N}(I_i, x_i, k)\right)$,

K is the number of Gaussian components, $\pi_{x_i,k}$ is the weight of the component k, I_i is the corresponding color vector of pixel i, $\mathcal{N}(I_i, x_i, k)$ is the Gaussian distribution of the component k.

$$E_{smooth} = \omega \sum_{i,j \in N} [x_i \neq x_j] \cdot \exp(-\gamma \|I_i - I_j\|^2),$$

ω is the weighting factor for normalizing penalties for color differences, N is the corresponding set of neighboring pixels, and the coefficient γ is a regulator of the intensity effect on the result.

When using the GrabCut algorithm, a Gaussian mixture model is built for the foreground and background at the E_{data} stage, preliminarily applying a threshold limit of values of 0.9 and 0.1, respectively, after which a new distribution is formed and combined with the results of the E_{smooth} component. Based on the results obtained, a graph is created with pixel vertices and weights of the probability of pixels belonging to a certain class. The min-cut technique of energy function optimization is used to divide the formed graph into two most independent parts of each other. The resulting graphs reflect the high accuracy of the segmentation of the input data into foreground and background due to the sequential iterative refinement of the Gaussian mixture model distribution parameters. In turn, this algorithm can create gaps in the middle of objects, so to enhance the integrity of the segmentation and remove small holes, the morphological closing operation was applied.

4. Results and Discussion

4.1. Dataset Description

The proposed computed tomography image segmentation technology based on the ResNet network integrated into the probabilistic model has been applied to three various datasets obtained from the Kaggle platform, which we will call COVID-19 [47], Chest [48], and Liver [49]. Each of the proposed datasets contains a series of computed tomography image frames and the corresponding region of interest segmentation objects (see Figs. 5, 6, and 7), namely 2729 frames in COVID-19, 2013 frames in the Chest, and 2324 frames in the Liver. All images are 512x512 pixels and are saved in JPEG and PNG formats.

Grayscale CT images often have low overall contrast – dark areas show particularly low contrast, while light areas tend to have high contrast. To define a preprocessing method that can improve the quality of grayscale CT images, a study was performed. Histogram equalization (HE), gamma correction (GAMMA), contrast limited adaptive histogram equalization (CLAHE), logarithmic intensity transformation (LOG), and Single Scale Retinex (SSR) methods have been applied to grayscale CT images distorted by Gaussian filters with various parameters.

To provide a numerical characterization of the image, the standard deviation of the brightness in an image (RMS contrast) was used: the higher the RMS, the higher the image contrast. To evaluate the effectiveness of the applied image enhancement methods, the mean squared error (MSE) between the enhanced and the original image is used. Table 1 shows results of applying image enhancement methods.

Table 1. Evaluation of Image Enhancement Methods.

RMS	Enhancement Methods				
	HE	GAMMA	CLAHE	LOG	SSR
	MSE ↓				
40.95	6177.01	2287.49	1621.99	11849.84	11936.03
58.01	1866.53	2011.45	1252.87	9448.74	6435.38
78.24	1250.46	1557.98	1411.57	7561.19	6335.03
91.68	4490.24	1065.44	1030.82	5150.58	5519.73

Experimental results show that the CLAHE method yields the lowest error among all evaluated techniques across different contrast variance ranges. This indicates its high effectiveness in preserving structural information and enhancing local contrast without significant distortions, making it one of the most suitable methods for improving the quality of medical images under varying contrast conditions.

The CLAHE algorithm in the proposed computed tomography image segmentation technology not only enhances an image and also ensures the system's resistance to distortions and artifacts. In turn, computed tomography images are a standardized type of medical data formed under normalized conditions and have low external influence from factors that generate noise and other artifacts.

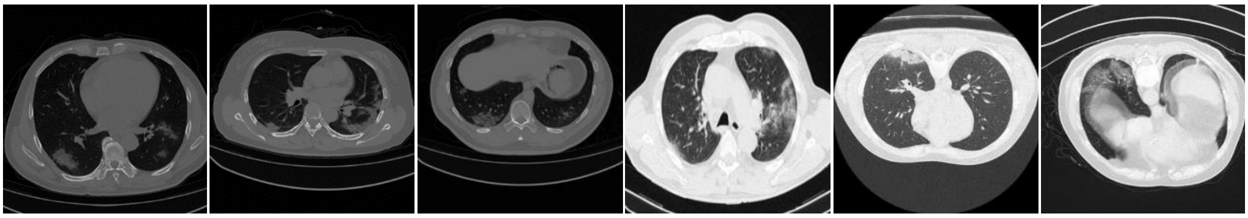

(a)

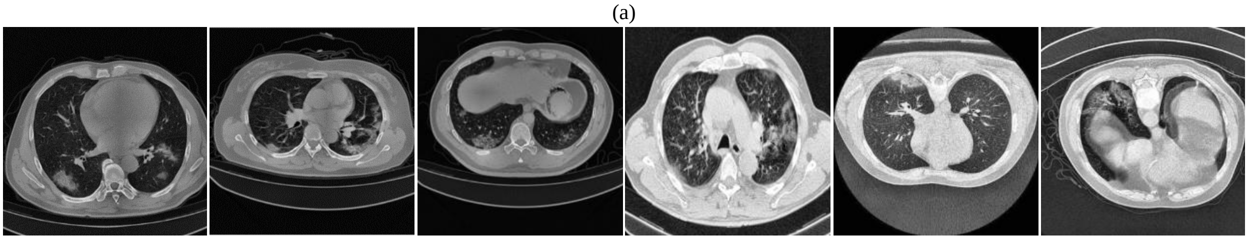

(b)

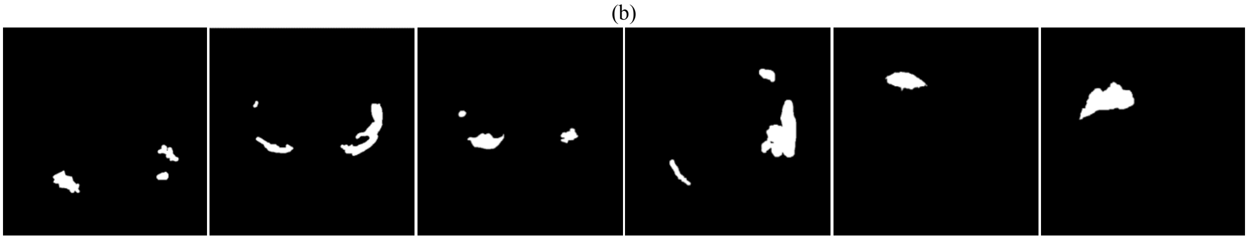

(c)

Fig. 5. Example images from the COVID-19 dataset: (a) original images; (b) contrast-enhanced images processed by CLAHE method; (c) original segmented regions.

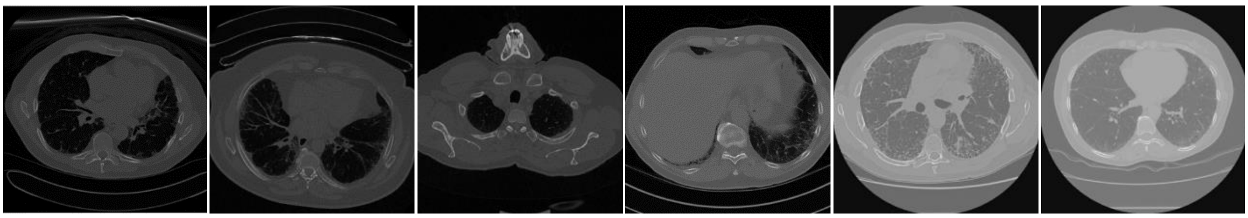

(a)

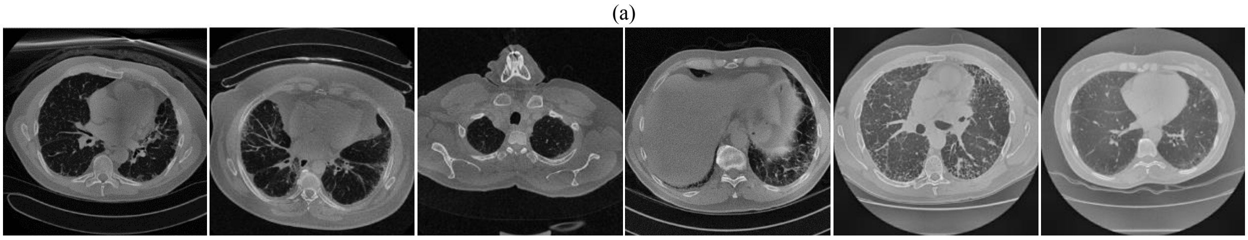

(b)

(c)

Fig. 6. Example images from the Chest dataset: (a) original images; (b) contrast-enhanced images processed by CLAHE method; (c) original segmented regions.

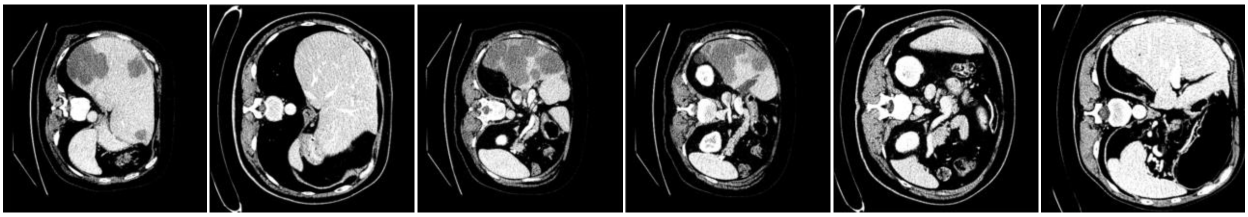

(a)

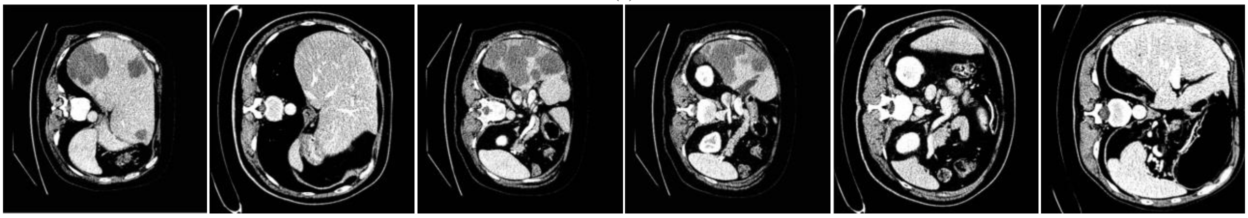

(b)

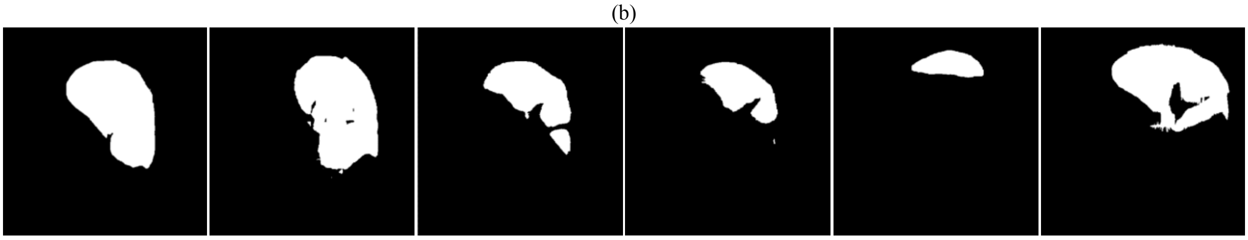

(c)

Fig. 7. Example images from the Liver dataset: (a) original images; (b) contrast-enhanced images processed by CLAHE method; (c) original segmented regions.

The object of interest in CT images (see Figs. 5, 6, and 7) can have a complex contour and structure, which further extends the segmentation process both in the COVID-19 dataset and smooth object contours, as in Chest or Liver. This dataset feature allows better evaluation of the proposed method's effectiveness on different data and comparing the results of segmentation accuracy evaluation.

When training the neural network models, the datasets were split into three corresponding image sets for training, validation, and testing with ratios of 75, 15, and 10 percent, respectively. So, for the COVID-19 dataset, the arrays of training, validation, and testing count 2046, 409, and 274 sets of CT image pairs and segmented regions, 1510, 300, and 203 sets for the Chest dataset, and 1744, 348, and 232 sets for the Liver dataset.

4.2. *Model Training and Validation*

The Adam optimizer, which uses an adaptive learning rate (10) with an ExponentialDecay scheduler to better tune the network's convergence was applied. This approach uses an exponential decay of the learning rate, which allows updating the weights more at the beginning of training and gradually reducing them to focus on fine-tuning the parameters.

$$lr = lr_0 \times (decay\_rate)^{\frac{step}{decay\_steps}}, \tag{10}$$

where $lr_0 = 0.001$, $decay\_rate = 0.96$, $decay_{steps} = 100000$ for the initial stages of learning.

A loss function combined with network architecture defines the performance of a deep learning model, in particular accuracy and reliability. Categorical Cross-Entropy loss, Dice loss, and Tversky loss functions have been applied for training the ResNet50 model. These loss functions have been chosen due to the SoftMax activation function in the last layer of the proposed ResNet50 model. Table 2 shows the results of applying loss functions to the proposed ResNet50 model. The training was performed on a data set limited to the 400 images.

Table 2. Evaluation of Loss Function Performance.

Loss Function	Evaluation Indicators				
	MSE ↓	IoU ↑	DSC ↑	Precision ↑	Recall ↑
Categorical Cross-Entropy	0.0035	0.6821	0.7821	0.8733	0.7380
Dice Loss	0.0056	0.5323	0.6276	0.6856	0.6233
Tversky Loss	0.0067	0.5323	0.6594	0.7352	0.6789

The impact of the Categorical Cross-Entropy loss function (11) on the performance of the proposed ResNet50 model was assessed.

$$L = -\frac{1}{M}\sum_{j=1}^{M}\sum_{i=1}^{C} y_{ji}\log(\widetilde{y_{ji}}), \quad (11)$$

where y is true of the pixel label; $\tilde{y}$ is the probability of belonging to class i; M is the number of instances in the batch, $M = 4$; C is the number of classes, $C = 2$.

At first the proposed ResNet50 model was trained on 50 epochs using the Adam optimizer with and without the adaptive learning rate to define the optimal epoch number. The results of training the proposed ResNet50 model are shown in Fig. 8.

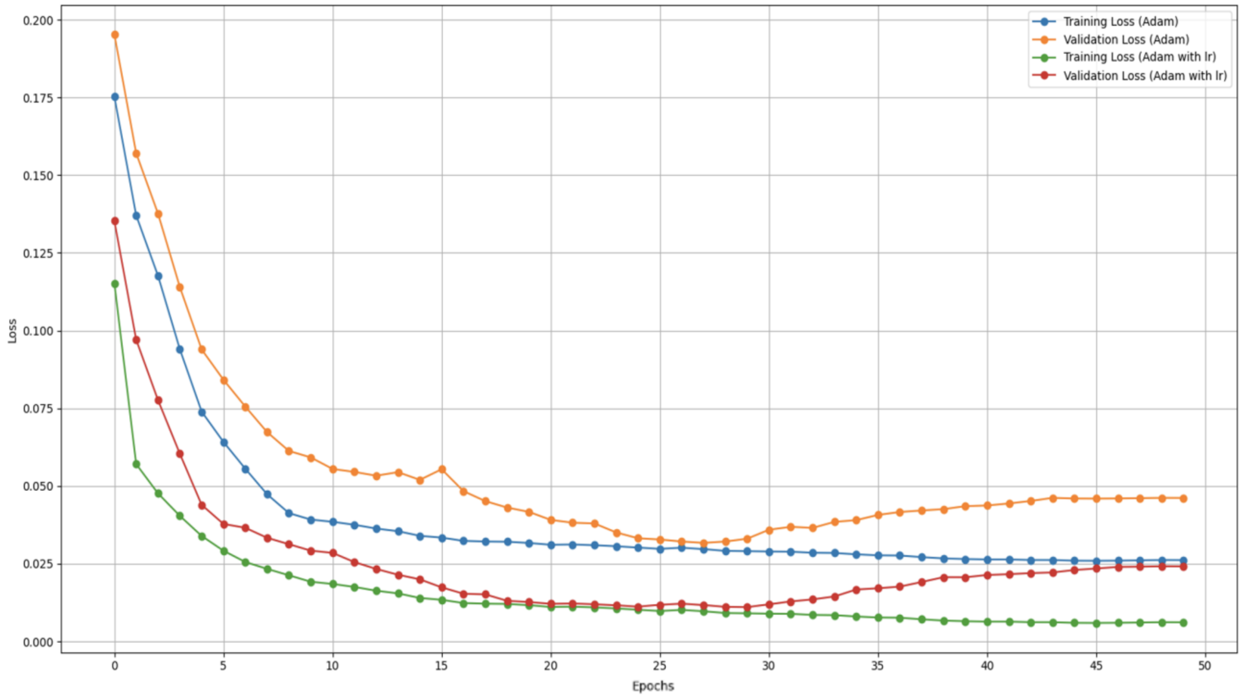

Fig. 8. Evolution of training and validation loss across 50 epochs.

Fig. 8 shows that after reaching the 30th epoch, the error rate on the validation data increases, which indicates overfitting of the system, which reduces the efficiency of using the proposed ResNet50 model. So, 30 epochs and Adam optimizer with an adaptive learning rate and the 30 epochs have been used to train the proposed ResNet50 model for achieving better network convergence.

According to Fig. 8, there is a possible risk of overfitting the model on the data. Therefore, a specialized training stop function was additionally used. This approach is known as Early Stopping. The EarlyStopping callback function of the TensorFlow framework monitors the modification of the validation loss parameter and stops the network training process if there is no improvement for three consecutive iterations. Fig. 9 shows training the proposed ResNet50 model using the Categorical Cross-Entropy loss function, Adam optimizer with an adaptive learning rate, and EarlyStopping callback function. The EarlyStopping callback function allowed speeding up the training process by reducing the number of epochs from 30 to 19, respectively.

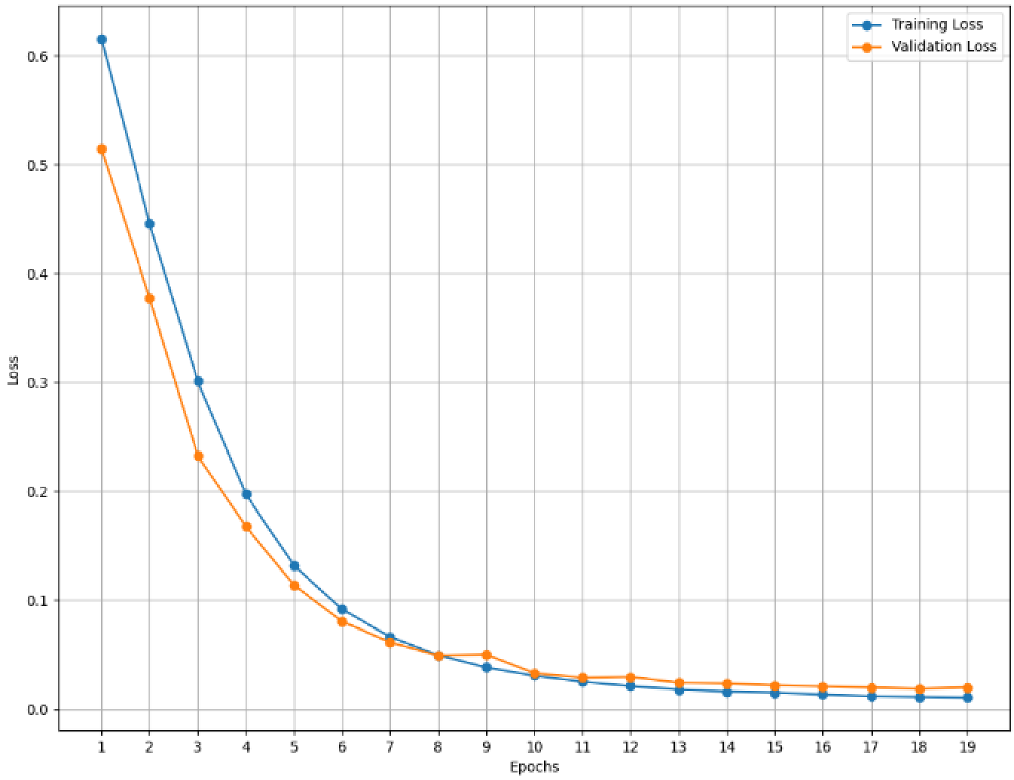

Fig. 9. Evolution of training and validation loss across 19 epochs.

The proposed computed tomography image segmentation technology has been performed on the Kaggle cloud platform using an NVIDIA TESLA P100 graphics processor, 16 GB of device memory, and 30 GB of RAM.

The duration of training the proposed ResNet50 model over 19 epochs using the specified hardware resources was 66 minutes. The response duration of the proposed ResNet50 model to segment the CT image was 0.08 second. The response duration of the proposed computed tomography image segmentation technology to segment the CT image was 0.082 second.

4.3. Evaluation Metrics

For assessing the accuracy of image segmentation, it is needed to decide quantitative criteria, which are widely used to evaluate the effectiveness of neural network models and other digital methods for medical image segmentation [50-51]. One of the principal terms used in segmentation accuracy metrics is True Positive (TP), which reflects the area where the guaranteed segmentation area overlaps with the area obtained by the method. False Positive (FP) reflects the segmentation area erroneously identified in the final result, and False Negative (FN) reflects the segmentation area erroneously excluded from the final result. Accordingly, the combination of these areas makes it possible to explore and evaluate the results of the method from different perspectives.

Thus, the Intersection over Union (12) and Dice Similarity Coefficient (13) enable the quantification of the similarity between the predicted method and the guaranteed segmentation. The precision (14) and the recall (15) enable determination of accuracy with which the proposed method determines the number of correctly identified pixels.

$$IoU = \frac{TP}{TP+FP+FN} \tag{12}$$

$$DSC = \frac{2 \times TP}{(TP+FP)+(TP+FN)} \tag{13}$$

$$Precision = \frac{TP}{TP+FP} \tag{14}$$

$$Recall = \frac{TP}{TP+FN} \tag{15}$$

Another quantitative metric is the root-mean-square error (16) of the number of corresponding correctly segmented pixels.

$$MSE = \frac{1}{n}\sum_{i=1}^{n}(y_i - \tilde{y}_i)^2 \tag{16}$$

For qualitatively assessing the accuracy of image segmentation, a survey was designed. In the survey, images from COVID-19, Chest, and Liver datasets were shown. Images in the survey have been segmented by the ResNet50 model and the proposed technology. A typical task has formed, "On slides images of the chest cavity. Image 1 is the original image. Image 2 is the segmentation result. Image 3 is the segmentation result''. Typical answer options were "The segments in image 2 are more accurate'', "The segments in image 3 are more accurate'', and "It is difficult to determine the more accurate segments''. The survey has been conducted among six respondents from radiological and surgical specializations.

4.4. Obtained Results and Analysis

The proposed computed tomography image segmentation technology based on the ResNet network integrated into the probabilistic model was applied to the CT chest images from the COVID-19, Chest, and Liver datasets. The segmentation results are shown in Figs. 10, 11, and 12.

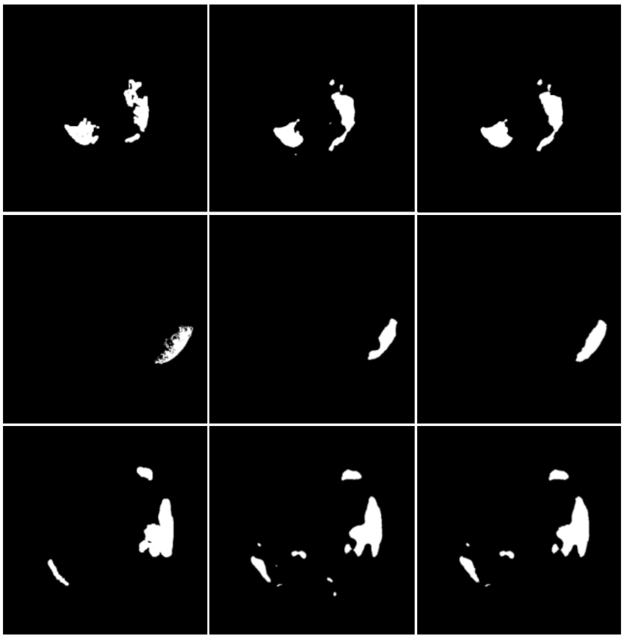

(a) (b) (c)

Fig. 10. Results of image segmentation for the COVID-19 dataset: (a) original segmented regions; (b) segmented regions detected by ResNet50; (c) segmented regions detected by the proposed image segmentation technology.

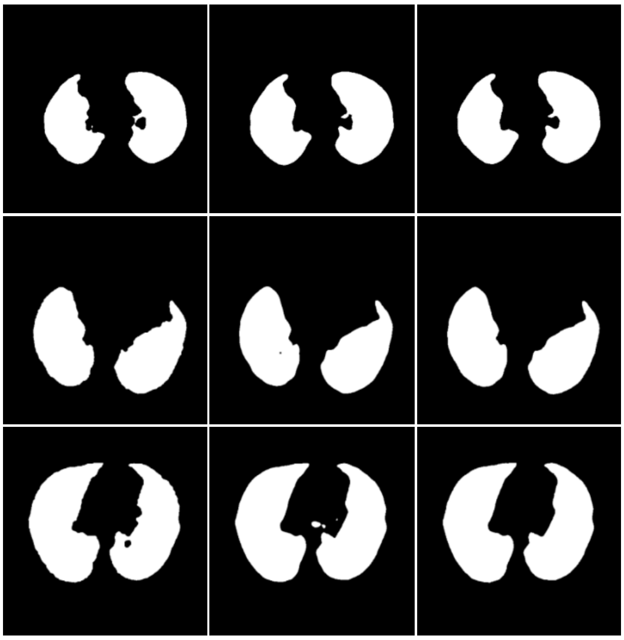

(a) (b) (c)

Fig. 11. Results of image segmentation for the Chest dataset: (a) original segmented regions; (b) segmented regions detected by ResNet50; (c) segmented regions detected by the proposed image segmentation technology.

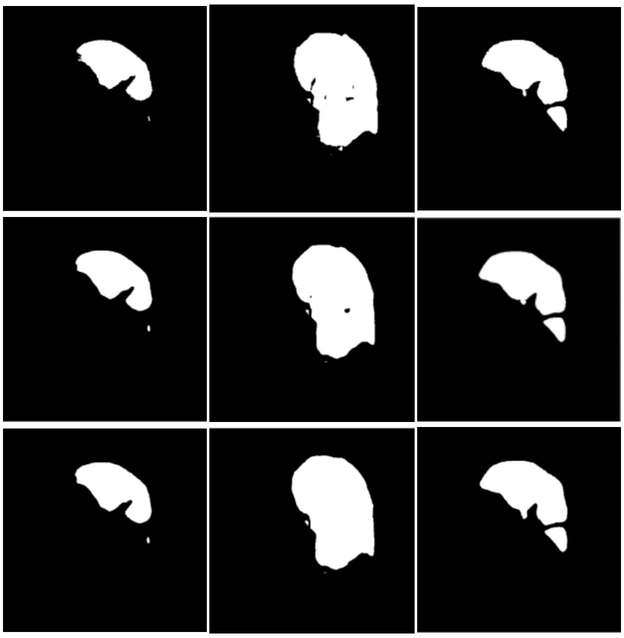

(a) (b) (c)

Fig. 12. Results of image segmentation for the Liver dataset: (a) original segmented regions; (b) segmented regions detected by ResNet50; (c) segmented regions detected by the proposed image segmentation technology.

Table 3 shows results of applying state-of-the-art technologies to segment the CT chest images for the COVID-19 dataset. Table 3 clearly demonstrates that when applying the proposed compound pooling block, the image segmentation accuracy is increased for all metrics except precision, that is, IoU improves by 5.16%, DSC by 5.15%, recall by 9.74%, and MSE by 0.29%. Table 3 confirms the effectiveness of using the proposed compound pooling block to consider the broader context of image objects.

Table 3. Evaluation of Deep Learning-Based Segmentation Methods for the COVID-19 dataset.

Method	Evaluation Indicators				
	IoU ↑	DSC ↑	Precision ↑	Recall ↑	MSE ↓
SegNet	0.3572	0.4750	0.5792	0.5221	0.0085
U-Net	0.4429	0.5574	0.6706	0.5278	0.0073
FCN-ResNet50	0.5625	0.6758	0.7848	0.6266	0.0068
FCN-ResNet50-Compound Pooling Block	0.6141	0.7273	0.7646	0.7240	0.0039

Table 4 shows results of applying state-of-the-art technologies and the proposed image segmentation technology to segment the CT chest images for the COVID-19 dataset. The proposed image segmentation technology provides the following values of segmentation accuracy: 61.87% by IoU, 73.12% by DSC, 75.01% by precision, 74.58% by recall, and 0.35% by MSE. Table 4 clearly demonstrates that when applying the proposed contextual block, the image segmentation accuracy is increased for all metrics except precision. On average, IoU improves by 0.85%, DSC by 0.78%, recall by 2.25%, and MSE by 0.27%, which is critically important for further data interpretation and analysis by a specialist.

Table 4. Evaluation of Deep Learning-Based Segmentation Methods and Proposed Contextual Block for the COVID-19 dataset.

Method	Evaluation Indicators				
	IoU ↑	DSC ↑	Precision ↑	Recall ↑	MSE ↓
SegNet-Contextual Block	0.3626	0.4831	0.5611	0.5368	0.0079
U-Net- Contextual Block	0.4541	0.5672	0.6559	0.5546	0.0071
FCN-ResNet50- Contextual Block	0.5751	0.6853	0.7717	0.6531	0.0062
Proposed Technology	0.6187	0.7312	0.7501	0.7458	0.0035

Table 5 and Table 6 show results of applying state-of-the-art technologies and the proposed image segmentation technology to segment the CT chest images for another dataset, namely Chest. Table 5 clearly demonstrates that when applying the proposed compound pooling block, the image segmentation accuracy is increased for all metrics except precision, and MSE remains unchanged, that is, IoU improves by 0.5%, DSC by 0.27%, and recall by 0.54%. Table 6 clearly demonstrates that when applying the proposed contextual block, the image segmentation accuracy is increased for all metrics except precision, and MSE is permanent. On average, IoU improves by 0.2%, DSC by 0.18%, and recall by 0.75%.

Table 5. Evaluation of Deep Learning-Based Segmentation Methods for the Chest dataset.

Method	Evaluation Indicators				
	IoU ↑	DSC ↑	Precision ↑	Recall ↑	MSE ↓
SegNet	0.9003	0.9315	0.9381	0.9301	0.0024
U-Net	0.9288	0.9573	0.9664	0.9524	0.0013
FCN-ResNet50	0.9514	0.9712	0.9806	0.9640	0.0010
FCN-ResNet50-Compound Pooling Block	0.9563	0.9739	0.9784	0.9694	0.0010

Table 6. Evaluation of Deep Learning-Based Segmentation Methods and Proposed Contextual Block for the Chest dataset.

Method	Evaluation Indicators				
	IoU ↑	DSC ↑	Precision ↑	Recall ↑	MSE ↓
SegNet-Contextual Block	0.9012	0.9327	0.9334	0.9363	0.0022
U-Net- Contextual Block	0.9312	0.9588	0.9621	0.9595	0.0011
FCN-ResNet50- Contextual Block	0.9533	0.9723	0.9779	0.9686	0.0009
Proposed Technology	0.9589	0.9771	0.9732	0.9815	0.0009

Table 6 clearly demonstrates that the proposed image segmentation technology has better segmentation accuracy than the state-of-the-art technologies; on average, IoU is 95.89%, DSC is 97.71%, recall is 98.15%, and MSE is 0.09%.

Table 7 and Table 8 show results of applying state-of-the-art technologies and the proposed image segmentation technology to segment the CT chest images for the Liver dataset. Table 7 clearly indicates that when applying the proposed compound pooling block, the image segmentation accuracy is increased for all metrics except precision, that is, IoU improves by 0.75%, DSC by 0.37%, recall by 0.45%, and MSE by 0.02%. Table 8 clearly demonstrates that when applying the proposed contextual block, the image segmentation accuracy is increased for all metrics except precision. On average, IoU improves by 0.17%, DSC by 0.1%, recall by 0.2%, and MSE by 0.02%.

Table 7. Evaluation of Deep Learning-Based Segmentation Methods for the Liver dataset.

Method	Evaluation Indicators				
	IoU ↑	DSC ↑	Precision ↑	Recall ↑	MSE ↓
SegNet	0.8923	0.9431	0.9404	0.9457	0.0011
U-Net	0.8962	0.9453	0.9482	0.9465	0.0019
FCN-ResNet50	0.9598	0.9795	0.9838	0.9802	0.0009
FCN-ResNet50-Compound Pooling Block	0.9673	0.9834	0.9821	0.9847	0.0007

Table 8. Evaluation of Deep Learning-Based Segmentation Methods and Proposed Contextual Block for the Liver dataset.

Method	Evaluation Indicators				
	IoU ↑	DSC ↑	Precision ↑	Recall ↑	MSE ↓
SegNet-Contextual Block	0.8924	0.9435	0.9412	0.9459	0.0011
U-Net- Contextual Block	0.9001	0.9479	0.9523	0.9485	0.0017
FCN-ResNet50- Contextual Block	0.9615	0.9804	0.9821	0.9847	0.0009
Proposed Technology	0.9677	0.9836	0.9809	0.9863	0.0007

Table 8 demonstrates that the proposed image segmentation technology has better segmentation accuracy than the state-of-the-art technologies; on average, IoU is 96.77%, DSC is 98.36%, recall is 98.63%, and MSE is 0.07%.

The survey results of respondents from radiological and surgical specializations and response percentages are shown in Table 9. Table 9 demonstrates that the proposed image segmentation technology improves the segmentation accuracy for computed tomography images.

Table 9. Segmentation accuracy survey results for the COVID-19, the Chest, and the Liver datasets.

Dataset	ResNet50 model, %	Proposed Technology, %	Cannot Decide, %
COVID-19	5.6	61.1	33.3
Chest	0	55.57	44.43
Liver	0	66.64	33.36

Therefore, applying the proposed computed tomography image segmentation technology based on the ResNet network integrated into the probabilistic model provides more accurate image segmentation results for both complex structure and contour (for example, the COVID-19 dataset) and a smooth structure of the object of interest (for example, the Chest and Liver datasets).

5. Conclusion and Future Research Directions

In this paper, the computed tomography image segmentation technology based on the ResNet network integrated into the probalistic model is proposed. The proposed image segmentation technology is based on deep learning-based segmentation and digital image processing-based segmentation to achieve high accuracy of object detection.

The proposed deep learning-based segmentation is based on the deep learning model of the ResNet50 architecture to extract features from images and detect objects. The ResNet50 network is based on the Compound Pooling block, which allows solving threats of losing image spatial information and relationships, which are critical for medical image analysis. Compared with the original FCN-ResNet50 deep fully convolutional neural network model, the proposed deep learning-based segmentation with the compound pooling block improves the segmentation accuracy by 5.16%, 5.15%, 9.74%, and 0.29% in terms of IoU, DSC, recall, and MSE for the COVID-19 dataset, by 0.5%, 0.27%, 0.54% for the Chest dataset, MSE remains unchanged, with improvements of 0.75%, 0.37%, 0.45%, 0.02% for the Liver dataset.

The proposed digital image processing-based segmentation is based on the contextual block, which allows capturing local features of the objects in a segmented ResNet50 image and the relationships between neighboring pixels by employing the probabilistic model with weighted parameters. The proposed probabilistic model is based on the integration of segmented images employing Conditional random fields, GrabCut algorithm, and argmax function on a segmented ResNet50 image. On average, the use of the proposed contextual block to refine the segmentation results of the neural network model provides an opportunity to improve the segmentation accuracy by 0.85%, 0.78%, 2.25%, and 0.27% in terms of IoU, DSC, recall, and MSE for the COVID-19 dataset, by 0.2%, 0.18%, and 0.75% for the Chest dataset, MSE remains unchanged, and by 0.17%, 0.1%, 0.2%, and 0.02% for the Liver dataset.

The computed tomography image segmentation technology based on ResNet network integrated into the probabilistic model increases the accuracy of the segmentation of medical images. According to the experimental data obtained according to the COVID-19 dataset, the proposed technology has a segmentation accuracy of 61.87% by the IoU, 73.12% by DSC, 75.01% by precision, 74.58% by recall, and 0.35% by MSE. Considering the Chest dataset, the proposed technology provides the following values of segmentation accuracy: 95.89% by IoU, 97.71% by DSC, 97.32% by precision, 98.15% by recall, and 0.09% by MSE. Considering the Liver dataset, the proposed technology provides the following values of segmentation accuracy: 96.77% by IoU, 98.36% by DSC, 98.09% by precision, 98.63% by recall, and 0.07% by MSE.

Medical image segmentation has a scarcity of expert-labeled data compared to other deep learning research fields. Therefore, augmenting medical expert-labeled data is primarily the easiest and fastest way to improve the deep learning model performance. Further research can be focused on performing the proposed computed tomography image segmentation technology based on the ResNet network integrated into the probabilistic model on other medical imaging datasets to evaluate its generalizability. To fully understand its capabilities, the technology should be evaluated on a wide array of datasets encompassing various medical conditions and imaging techniques. For example, datasets related to brain imaging (computed tomography and/or magnetic resonance imaging) can demonstrate perspectives of providing the proposed image segmentation technology based on the ResNet network integrated into the probabilistic model in diverse medical domains.

Further research can be focused on exploring the impact of tuning weighted parameters of the proposed probabilistic model on the performance of the proposed image segmentation technology. As a result, it will be necessary to develop an adaptive method of applying the proposed contextual block to deep learning-based segments.

References

[1] O. Ronneberger, P. Fischer, T. Brox, “UNet: Convolutional networks for biomedical image segmentation,” in *Proceedings of the International Conference on Medical Image Computing and Computer-Assisted Intervention, Munich, Germany, 5–9 October 2015*, pp. 234–241, 2015.

[2] L.C. Chen, G. Papandreou, I. Kokkinos, K. Murphy, A.L. Yuille, “DeepLab: semantic image segmentation with deep convolutional nets, atrous convolution, and fully connected CRFs,” *IEEE Transactions on Pattern Analysis and Machine Intelligence*, pp. 834–848, 2018.

[3] V. Badrinarayanan, A. Handa, R. Cipolla, “SegNet: A deep convolutional encoder–decoder architecture for robust semantic pixel-wise labelling,” *arXiv:1505.07293*, 2015.

[4] U.F. Mohammad, M. Almekkawy, “Automated detection of liver steatosis in ultrasound images using convolutional neuralnetworks,” in *Proceedings of the 2021 IEEE International Ultrasonics Symposium China, 11–16 September 2021*, pp.1-4, 2021.

[5] C. Peng, X. Zhang, G. Yu, G. Luo, J. Sun, “Large kernel matters – Improve semantic segmentation by global convolutional network,” in *Proceedings of the IEEE Conference on Computer Vision and Pattern Recognition,* pp. 4353–4361, 2017.

[6] J. Long, E. Shelhamer, and T. Darrell, “Fully convolutional networks for semantic segmentation,” in *Proceedings of the IEEE Conference on Computer Vision and Pattern Recognition*, pp. 3431–3440, 2015.

[7] J. Chen, Y. Lu, Q. Yu, X. Luo, E. Adeli, Y. Wang, L. Lu, A. L. Yuille, Y. Zhou, “TransUNet: Transformers make strong encoders for medical image segmentation,” *arXiv:2102.04306*, 2021.

[8] H. Cao, Y. Wang, J. Chen, D. Jiang, X. Zhang, Q. Tian, M. Wang, “SwinUNet: UNet-like pure transformer for medical image segmentation,” *arXiv:2105.05537*, 2021.

[9] W. Chen, Y. Wang, D. Tian, Y. Yao, “CT Lung Nodule Segmentation: A Comparative Study of Data Preprocessing and Deep Learning Models,” *IEEE Access*, Vol.23, pp. 34925-34931, 2023.

[10] M. Heidari, S. Mirniaharikandehei, A. Z. Khuzani, G. Danala, Y. Qiu, B. Zheng, “Improving the performance of CNN to predict the likelihood of COVID-19 using chest X-ray images with preprocessing algorithms,” *International Journal of Medical Informatics*, Vol. 144, 2020.

[11] H. Zanddizari, N. Nguyen, B. Zeinali, J.M. Chang, “A new preprocessing approach to improve the performance of CNN-based skin lesion classification,” *Medical Biological Engineering Computing*, Vol. 59, pp. 1123-1131, 2021.

[12] H. Huang, L. Lin, R. Tong, H. Hu, Q. Zhang, Y. Iwamoto, X. Han, Y.W. Chen, J. Wu, “UNet 3+: A full-scale connected UNetfor medical image segmentation,” in *Proceedings of the ICASSP 2020—2020 IEEE International Conference on Acoustics, Speechand Signal Processing (ICASSP), Barcelona, Spain, 4–8 May 2020*, pp. 1055–1059, 2020.

[13] L.-C. Chen, Y. Zhu, G. Papandreou, F. Schroff, H. Adam, “Encoder-decoder with atrous separable convolution for semantic image segmentation,” in *Proceedings of the 15th European Conference, Munich, Germany, September 8–14, 2018*, pp. 801-818, 2018.

[14] Z. Xiao, M. Du, J. Liu, E. Sun, J. Zhang, X. Gong, Z. Chen, “EA-UNet based segmentation method for OCT image of uterine cavity,” *Photonics*, Vol. 10(1), 2023.

[15] A.H. Alwan, S.A. Ali, A.T. Hashim, “Medical image segmentation using enhanced residual U-Net architecture,” *Mathematical Modelling of Engineering Problems*, Vol.11, No.2, pp. 507-516, 2024.

[16] V. Jumutc, D. Bliznuks, A. Lihachev, “Multi-Path UNet architecture for cell and colony-forming unit image segmentation,” *Sensors*, Vol. 22, 2022.

[17] X. Chen, L. Yao, Y. Zhang, “Residual attention u-net for automated multi-class segmentation of covid-19 chest CT images,” *arXiv:2004.05645*, 2020.

[18] S. Tao, Y. Jiang, S. Cao, C. Wu, Z. Ma, “Attention-guided network with densely connected convolution for skin lesionsegmentation,” *Sensors*, Vol. 21, 2021.

[19] A. Khan, R. Garner, M.L. Rocca, S. Salehi, D. Duncan “A novel threshold-based segmentation method for quantification of COVID-19 lung abnormalitie,” *Signal, Image and Video Processing*, Vol.17, pp. 907-914, 2023.

[20] L. Abualigah, A. Diabat, P. Sumari, A.M. Gandomi, “A novel evolutionary arithmetic optimization algorithm for multilevel thresholding segmentation of COVID-19 CT images,” *Evolutionary Process for Engineering Optimization*, Vol. 9, 2021.

[21] Z. Zhou, Z. Xue-chang, Z. Si-ming, X. Hua-fei, S. Yue-ding, “Semi-automatic liver segmentation in CT images through intensity separation and region growing,” *Procedia computer science*, Vol. 131, pp. 220-225, 2018.

[22] A. Khorshidi, J. Soltani-Nabipour, B. Noorian, “Lung tumor segmentation using improved region growing algorithm,” *Nuclear Engineering and Technology*, Vol. 52, No. 10, pp. 2313-2319, 2020.

[23] O. Shkurat, Y. Sulema Y., V. Suschuk-Sliusarenko, A. Dychka, “Image Segmentation Method Based on Statistical Parameters of Homogeneous Data Set,” *Advances in Intelligent Systems and Computing*, Vol. 902, pp. 271–281, 2020.

[24] B. Rim, S. Lee, A. Lee, H.-W. Gil, M. Hong, “Semantic cardiac segmentation in chest CT images using K-means clustering and the mathematical morphology method,” *Computer Vision and Machine Learning for Medical Imaging System*, Vol. 21, 2021.

[25] J. Kong, J. Hou, M. Jiang, J. Sun, “A novel image segmentation method based on improved intuitionistic fuzzy C-means clustering algorithm,” *KSII Transactions on Internet and Information Systems,* Vol. 13, No.6, pp. 3121–3143, 2019.

[26] M. S. Alam, M. K. Islam, M. S. Ali, M. S. Miah, M. M. Rahman, M. A. Hossain, “Brain tumor detection in MR image using superpixels, principal component analysis and template based K-means clustering algorithm,” *Machine Learning with Applications*, Vol. 5, 2021.

[27] E. E. Nithila, S. S. Kumar, “Segmentation of lung nodule in CT data using active contour model and Fuzzy C-mean clustering,” *Alexandria Engineering Journal*, vol. 55, no. 3, pp. 2583-2588, 2016.

[28] W. Wu, S. Wu, Z. Zhou, R. Zhang and Y. Zhang, “3D liver tumor segmentation in CT images using improved fuzzy C□means and graph cuts,” *BioMed Research International*, Vol. 2017, No. 1, 2017.

[29] A. Zareei, A. Karimi, “Liver segmentation with new supervised method to create initial curve for active contour,” *Computers in Biology and Medicine,* Vol. 75, pp. 139-150, 2016.

[30] Q. Huang, H. Ding, X. Wang, G. Wang, “Fully automatic liver segmentation in CT images using modified graph cuts and feature detection,” *Computers in biology and medicine*, Vol. 95, pp. 198-208, 2018.

[31] J. Wang, Y. Cheng, C. Guo, Y. Wang, S. Tamura, “Shape-intensity prior level set combining probabilistic atlas and probability map constrains for automatic liver segmentation from abdominal CT images,” *International journal of computer assisted radiology and surgery*, Vol. 11, pp. 817–826, 2016.

[32] B. A. Skourt, A. El Hassani, A. Majda, "Lung CT image segmentation using deep neural networks," *Procedia Computer Science*, Vol. 127, pp. 109-113, 2018.
[33] P. F. Christ, F. Ettlinger, F. Grün, J. Lipkova, S. Schlecht, B. Menze, et al "Automatic liver and tumor segmentation of CT and MRI volumes using cascaded fully convolutional neural networks," *arXiv:1702.05970*, 2017.
[34] P. F. Christ, F. Ettlinger, S. Tatavarty, M. Bickel, P. Bilic, B. Menze, et al "Automatic liver and lesion segmentation in CT using cascaded fully convolutional neural networks and 3D conditional random fields," *arXiv:1610.02177*, 2016.
[35] C. Sun, S. Guo, H. Zhang, J. Li, M. Chen, S. Ma, et al, "Automatic segmentation of liver tumors from multiphase contrast-enhanced CT images based on FCNs," *Artificial intelligence in medicine*, Vol. 83, pp 58-66, 2017.
[36] B. Cai, Q. Xu, C. Yang, Y. Lu, C. Ge, Z. Wang, et al, "Spine MRI image segmentation method based on ASPP and U-Net network," *Mathematical Bioscience and Engineering*, Vol. 20, No. 9, pp. 15999-16014, 2023.
[37] P. V. Nayantara, S. Kamath, R. Kadavigere, K. N. Manjunath, "Automatic Liver Segmentation from Multiphase CT Using Modified SegNet and ASPP Module," *SN Computer Science*, Vol. 5, No. 4, 2024.
[38] K. Kamnitsas, C. Ledig, V. F. Newcombe, J. P. Simpson, A. D. Kane, B. Glocker, et al, "Efficient multi-scale 3D CNN with fully connected CRF for accurate brain lesion segmentation," *Medical Image Analysis*, Vol. 36, pp. 61-78, 2016.
[39] W. Zhang, Y. Tao, W. Liang, J. Li, Y. Chen, T. Song, et al, "Automatic segmentation of liver tumor from multi-phase contrast-enhanced CT images using cross-phase fusion transformer," *Asian-Pacific Conference on Medical and Biological Engineering*, Vol. 103, pp. 121-130, 2024.
[40] X. Xie, W. Zhang, H. Wang, L. Li, Z. Feng, Z. Wang, et al, "Dynamic adaptive residual network for liver CT image segmentation," *Computers & Electrical Engineering*, Vol. 91, 2021.
[41] P. Dutande, U. Baid, S. Talbar, "Deep residual separable convolutional neural network for lung tumor segmentation," *Computers in Biology and Medicine*, Vol. 141, 2022.
[42] R. V. Manjunath, Y. Gowda, H. M. Manu, "Automated liver segmentation from CT images using modified ResUNet," *Gastroenterology & Endoscopy*, Vol. 3, pp. 93-104, 2025.
[43] A. Ilhan, K. Alpan, B. Sekeroglu, R. Abiyev, "COVID-19 Lung CT image segmentation using localization and enhancement methods with U-Net," *Procedia Computer Science*, Vol. 218, pp.1660-1667, 2023.
[44] Li L., Si Y., Jia, Z. (2018). Medical image enhancement based on CLAHE and unsharp masking in NSCT domain. Journal of Medical Imaging and Health Informatics, 8(3), 431-438.
[45] K. He, X. Zhang, S. Ren, J. Sun, "Deep Residual Learning for Image Recognition," *arXiv:1512.03385*, pp. 770-778, 2015.
[46] P. Krähenbühl, V. Koltun, "Efficient inference in fully connected crfs with gaussian edge potentials," *arXiv:1210.5644*, 2011.
[47] COVID-19 dataset: https://www.kaggle.com/datasets/maedemaftouni/covid19-ct-scan-lesion-segmentation-dataset.
[48] Chest dataset: https://www.kaggle.com/datasets/polomarco/chest-ct-segmentation.
[49] Liver dataset: https://www.kaggle.com/datasets/ag3ntsp1d3rx/litsdataset2/data.
[50] S. Winzeck, A. Hakim, R. McKinley, J. A. Pinto, V. Alves, C. Silva, et al., "ISLES 2016 and 2017-benchmarking ischemic stroke lesion outcome prediction based on multispectral MRI," *Frontiers in neurology*, Vol. 9, p. 679, 2018.
[51] L. Weninger, O. Rippel, S. Koppers and D. Merhof, "Segmentation of Brain Tumors and Patient Survival Prediction: Methods for the BraTS 2018 Challenge," in *Brainlesion: Glioma, Multiple Sclerosis, Stroke and Traumatic Brain Injuries*, Vol 11384, pp. 3-12, 2019.

Authors' Profiles

Zhengbing Hu, Prof., Deputy Director, International Center of Informatics and Computer Science, Faculty of Applied Mathematics, National Technical University of Ukraine "Igor Sikorsky Kyiv Polytechnic Institute", Ukraine. Adjunct Professor, School of Computer Science, Hubei University of Technology, China. Visiting Prof., DSc Candidate at the National Aviation University (Ukraine) from 2019. Major research interests: Computer Science and Technology Applications, Artificial Intelligence, Network Security, Communications, Data Processing, Cloud Computing, Education Technology.

Kostiantyn Zvieriev, Master's student at the Department of Computer Systems Software of the Faculty of Applied Mathematics at the Igor Sikorsky Kyiv Polytechnic Institute. Research interests: Data and Image Processing, Methods and Algorithms for Process Optimization, Construction of Automated Computer Systems.

Oksana Shkurat, Assistant Professor at the Department of Computer Systems Software of the Faculty of Applied Mathematics at the Igor Sikorsky Kyiv Polytechnic Institute. Research interests: Image Processing Technology, Computer Vision Technology, Artificial Intelligence.

Andrii Dychka, Assistant at the Department of Computer Systems Software of the Faculty of Applied Mathematics at the Igor Sikorsky Kyiv Polytechnic Institute. Research interests: Barcoding, Multicolor Barcodes, Data Processing.

How to cite this paper: Zhengbing Hu, Kostiantyn Zvieriev, Oksana Shkurat, Andrii Dychka, "Computed Tomography Image Segmentation Technology Based on ResNet Network Integrated into the Probabilistic Model", International Journal of Image, Graphics and Signal Processing(IJIGSP), Vol.17, No.4, pp. 14-32, 2025. DOI:10.5815/ijigsp.2025.04.02